

Hyperelastic swelling of tough hydrogels

Jing Wang and Justin C. Burton*
Department of Physics, Emory University.
 (Dated: January 10, 2024)

Hydrogels are biphasic, swollen polymer networks where elastic deformation is coupled to nanoscale fluid flow. As a consequence, hydrogels can withstand large strains and exhibit non-linear, hyperelastic properties. For low-modulus hydrogel and semiflexible biopolymer networks, previous studies have shown that these materials universally contract when sheared on timescales much longer than the poroelastic relaxation timescale. Using rheological and tribological measurements, we find that tough polyacrylamide and polyacrylic acid hydrogels, with moduli of order ~ 10 -100 kPa, exclusively exhibit dilatancy when sheared. The poroelastic relaxation process was examined using strain-controlled compression, indicating a diffusion constant of order 10^{-9} m²/s. On short timescales (minutes), an applied shear stress induced an increase in normal stress that varied quadratically with shear strain. At long timescales (hours), creep experiments revealed that tough hydrogels can “remember” the initial direction of applied shear, suggesting an evolution of the polymer network. Moreover, we show that this dilatant behavior manifests as swelling during tribological sliding, imbibing the hydrogel with fluid. We suggest that this inherent, hyperelastic dilatancy is an important feature in all tough hydrogels, and may explain rehydration and mechanical rejuvenation in biological tissues such as cartilage.

I. INTRODUCTION

Hydrogels exhibit complex, time-dependent mechanical properties due to their biphasic nature. Material deformation inherently requires the solvent to flow relative to the underlying cross-linked polymer matrix. In recent years, hydrogels have been engineered and investigated for applications such as urban farming [1], cosmetic care [2, 3], tissue engineering [4, 5], and drug delivery [6–8]. In particular, tough hydrogels with a Young’s modulus > 10 kPa exhibit ultra-low friction and have been used as a model system for articular cartilage [9–14]. Recent tribological experiments show an increase of cartilage (hydrogel) volume upon sliding at a smooth interface, a process attributed to “tribological rehydration” [15–20]. The rehydration process is velocity-dependent and is claimed to only occur at the hydrogel contact interface as a result of the competition between elastohydrodynamic pressure inflow and interstitial pressure outflow [21]. In this sense, the application of shear (through mechanical motion, i.e., joint activity) will imbibe the cartilage with fluid, softening and rejuvenating the tissue.

Alternatively, here we will show that rejuvenation and swelling of tough hydrogels can be ascribed to their bulk, hyperelastic mechanical properties. Specifically, the Poynting effect, which describes the development of stress perpendicular to the direction of shear in a confined elastic material [22–24]. The Poynting effect has been observed in materials such as rubber [25], metal wires [22], soft fiber materials [26, 27], soft polymer gels [28, 29], and emulsions [30]. The normal stress, σ_N , in hyperelastic materials is captured by the Mooney-Rivlin model [31, 32], which predicts that when sheared at a fixed volume, $\sigma_N \propto \gamma^2$, where γ is the shear strain. The effect

can be positive (dilatant) or negative (contractile). In 2007, Janmey *et al.* [33] first reported contractile behavior in semiflexible biopolymer gels such as fibrin, which has been confirmed by subsequent studies [34–37]. However, Janmey *et al.* [33] also reported a dilatant behavior in low-modulus, weakly-cross-linked polyacrylamide (PAAm) hydrogels. While this was attributed to the flexibility of the polymers, instead de Cagny *et al.* [38] revealed that poroelastic flow on long timescales can alter the sign of the normal stress response, so that an initial dilatant behavior can transition to a contractile one in PAAm with moduli of order ~ 100 Pa. They further suggested that any confined hydrogel would eventually exhibit negative normal stress in response to shear after sufficient waiting time. However, here we show tough hydrogels with moduli of order 10-100 kPa *always* exhibit dilatant, hyperelastic behavior, even after the fluid flow has decoupled from the network at long times.

Both contractile and dilatant responses in hydrogels can be predicted based on the change in shear modulus under compression. Following Tighe *et al.* [39, 40], when sheared under constant volume, the normal stress response of an elastic solid can be expressed as

$$\Delta\sigma_N = \frac{1}{2}R_v\gamma^2 + \mathcal{O}(\gamma^4), \quad (1)$$

where R_v is the Reynolds coefficient at a fixed volume:

$$R_v = E \left(\frac{\partial G}{\partial \sigma_N} \right)_\gamma - G. \quad (2)$$

Here, G is the shear modulus, E is the Young’s modulus, and the subscript γ implies that the derivative is taken at constant, infinitesimal shear strain. Generally, $G < E$, and the material will exhibit dilatant behavior if the differential in the first term is large enough and positive. For granular packings, $\partial G / \partial \sigma_N > 0$, as evidenced by studies of dilatancy in granular materials dating back to 1886 [41], and more recently in a broader class

* justin.c.burton@emory.edu

of granular materials such as emulsions [30]. For spring networks, often used as a minimal model for cross-linked gels, $\partial G/\partial \sigma_N < 0$, implying that spring networks universally contract upon compression [40]. As mentioned, contractile behavior is indeed observed in semi-flexible biopolymer networks and weakly cross-linked hydrogels [33, 38].

We have conducted a series of both surface tribological sliding and bulk rheological shearing experiments using tough PAAm hydrogels. These hydrogels exclusively dilate in all experiments, in contrast to low modulus gels and the expected behavior of network materials. We first characterized the poroelastic diffusion of the hydrogel network upon compression in order to decouple fluid transport from rheological response. We then illustrate how dilatant behavior is manifested in confined and unconfined tribological sliding experiments. We also used low-amplitude oscillatory shear to directly measure R_v , and show that Eqn. 2, which is derived from a purely elastic solid, is a reasonable estimate to the dilatant behavior.

Finally, we used high-amplitude oscillatory shear and multi-day creep experiments to illustrate how the dilatant behavior of tough hydrogels deviates from simple, quadratic models of hyperelasticity (Eqn. 1) over long times due to irreversible, plastic deformation. These results provide a natural explanation for the volumetric expansion of cartilage during sliding, and are applicable to a broader class of tough synthetic hydrogels and biological tissues.

II. DIFFUSION-DRIVEN RELAXATION

The hyperelastic response of hydrogels can change in both magnitude and sign during poroelastic relaxation [38]. This process is driven by the relative diffusion of the solvent and polymer network, as described by Doi *et al.* [42, 43]. The diffusion constant can be written as

$$D = \frac{Ek(1-\nu)}{\mu(1+\nu)(1-2\nu)}, \quad (3)$$

where E is the Young's modulus of the hydrogel, k is the permeability, μ is the viscosity of the solvent (water), and ν is Poisson's ratio [44]. For the PAAm and PAA (polyacrylic acid) hydrogel spheres used in our experiments (see SI), $E \approx 35.7$ kPa (Fig. S1), $\nu \approx 0.40$, and $k \propto \xi^2$, where $\xi \approx 5 - 15$ nm is the mesh size of the polymer network [45]. Thus we expect $D \approx 2 - 20 \times 10^{-9}$ m²/s.

We characterized the diffusion process in our hydrogels by examining the relaxation of the normal force under compression using a rheometer (AR 2000, TA Instruments). With a 60-mm parallel plate geometry, hydrogel spheres were compressed on top of a plano-concave lens fully immersed in a water bath (Fig. 1B inset). A custom solvent trap was placed on top of the water bath to prevent evaporation over day-long timescales. Each experiment began by applying a constant normal force,

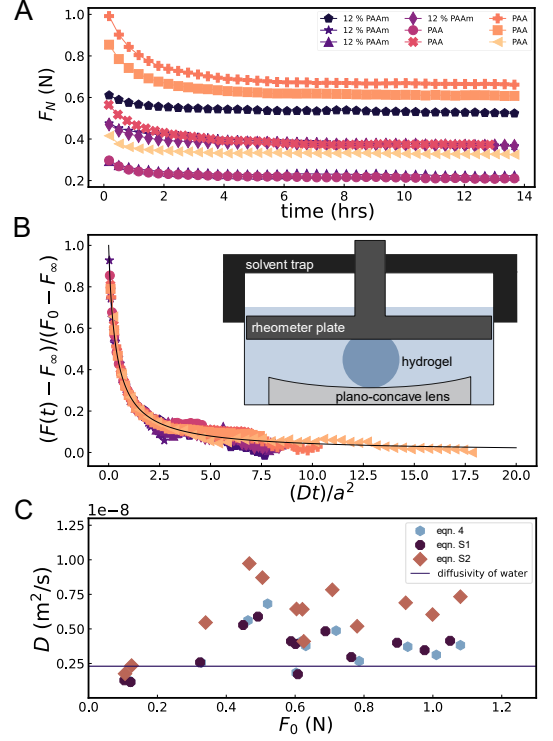


FIG. 1. Tough hydrogels display poroelastic relaxation upon compression. (A) Under fixed strain, the applied normal force relaxed to a constant value after many hours. (B) Assuming a diffusive relaxation process (Eqn. 4, SI Eqn. 1 and 2), the data can be collapsed by scaling both axes. Inset: experimental schematic showing a hydrogel sphere (diameter ≈ 1.5 cm) compressed in a rheometer and left to relax under constant normal strain. The concave lens ensured centering of the gel. (C) The extracted diffusion constant was independent of the exact fitting form, and comparable to the self-diffusivity of water (solid line).

F_0 , which determined the amount of compressive normal strain ($\approx 1 - 10\%$). We subsequently recorded the normal force response, $F_N(t)$, during relaxation for 14 hours. The normal strain (determined by the rheometer gap size) remained constant during the experiment. Figure 1A shows $F_N(t)$ for commercial PAA and 12 % PAAm spheres with different levels of initial compression.

In all cases, $F_N(t)$ decreased rapidly at early times but eventually reached a plateau at late times. This behavior agrees with numerous previous studies using indentation methods such as the atomic force microscopy to study hydrogel poroelasticity [15, 46–50].

The data in Fig. 1A can be collapsed onto a single curve by scaling the vertical and horizontal axes. The initial and final values of the force determine the vertical axis scaling, whereas time is scaled by $\tau = a^2/D$, where D should be the diffusion constant (Eqn. 3). The contact area a was measured using particle exclusion microscopy as described in Ref. [45]. The diffusion constant can be

found by fitting the data to a functional form that can capture the relaxation dynamics [46, 47]. To collapse the data in Fig. 1A, we used the following function, taken from Berry *et al.* [46]:

$$\frac{F_N(t) - F_\infty}{F_0 - F_\infty} = 1 - \frac{2.56(Dt/a^2)^{0.94}}{1 + 2.56(Dt/a^2)^{0.94}}, \quad (4)$$

where $F_\infty = F_N(t = \infty)$. This function is empirical, and we found that other fitting functions provide similar results, as described in the SI. Since a is measured by microscopy, the fitting parameters were D , F_0 , and F_∞ . The collapsed data is shown in Fig. 1B. The extracted diffusion constants (D) using Eqn. 4, Eqn. S1, and Eqn. S2 are shown in Fig. 1C as a function of the initial compressive force, F_0 . The values of D ranged from $1.2 - 9.7 \times 10^{-9} \text{ m}^2/\text{s}$, which is consistent with the estimate from Eqn. 3. We note that our measurements are 10-100 times larger than values of D reported from micro-indentation measurements on hydrogel surfaces [46, 50]. Despite this discrepancy, we also note excellent agreement with values of D extracted from swelling experiments of similar-sized hydrogel particles [44].

III. TRIBOLOGICAL SWELLING

Without confinement, tough hydrogels will swell in response to an imposed shear stress, for example, frictional sliding against a smooth surface. The shear stress applied at the sliding interface is transmitted into the bulk, resulting in hyperelastic swelling. This effect also manifests as increased normal stress in confined environments. In fully-relaxed, compressed hydrogel spheres, we observed sliding-induced swelling using stress-controlled tribology experiments and strain-controlled rheology experiments.

Figure 2 inset shows our custom-built tribometer [45, 51]. Hydrogel spheres were compressed onto an acrylic surface with a constant normal load of $F_N = 0.2 \text{ N}$. A spot was marked above the hydrogel sphere and its vertical position was recorded at 1 frame per second and tracked using image analysis. The time evolution of the vertical displacement is depicted in Fig. 2. We define $t = 0 \text{ hrs}$ when the normal load was first applied to the hydrogel sphere. For $0 < t < 10 \text{ hrs}$, the displacement displayed relaxation to equilibrium, similar to the normal force relaxation Fig. 1A. At $t = 10 \text{ hrs}$, a constant sliding velocity of 1 cm/s was applied for 3 hrs . The vertical displacement increased rapidly by $70 \mu\text{m}$ and ultimately reached a plateau. Importantly, upon cessation of sliding at $t = 13 \text{ hrs}$, the vertical displacement continued to relax from the plateau with a similar timescale as the initial relaxation. This demonstrates that swelling occurred over the bulk of the material and not simply at the interface.

In confined environments, the dilatancy of tough hydrogels under shear or sliding will lead to an increase normal force. To show this, we used strain-controlled

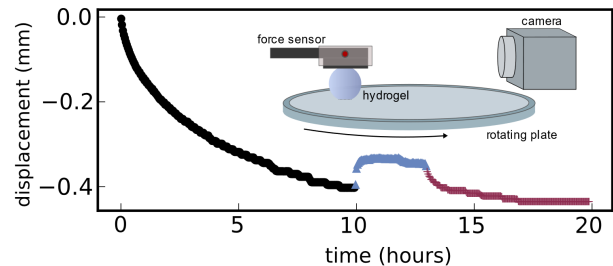


FIG. 2. Tough hydrogels swell during tribological sliding. Plotted data represents vertical displacement vs. time during the initial compression ($t < 10 \text{ hrs}$), during sliding at 1.0 cm/s ($10 \text{ hrs} < t < 13 \text{ hrs}$), and post sliding ($t > 13 \text{ hrs}$). The contact radius of the PAA sphere was $\approx 3 \text{ mm}$ under a normal load of 0.2 N . The inset shows an illustration of the stress-controlled tribology setup for displacement imaging. The relaxation and swelling of the hydrogel was monitored by tracking the position of the red circle on the apparatus. A thin layer of water was used to ensure hydration of hydrogel spheres.

rheology with PAA commercial hydrogel spheres, as depicted in Fig. 3C inset. An aluminum plate (diameter = 60 mm) with 3 divots was glued to the top parallel plate of the rheometer. The divots were placed at the vertices of an equilateral triangle, each 20 mm from the plate center. A small amount of modeling clay was used in the divots to prevent undesired rolling of the spheres. Sliding occurred at a smooth acrylic surface at the bottom of each sphere. An initial normal force of $F_0 = 0.9 \text{ N}$ was applied to compress the hydrogel spheres for 8 hours . Subsequently, the sliding velocity (v) was ramped logarithmically from 0.06 to 60 cm/s , spending 180 s at each velocity. Hydrogel spheres were additionally monitored for 4.5 hours post sliding. The gap size remained constant throughout the experiment, corresponding to a normal strain of 3% . The normal force F_N , shear force F_S , and the coefficient of friction $\mu = F_S/F_N$ are shown in Fig. 3A, 3B, and 3C, respectively.

Upon initial compression, the normal force relaxed identically to Fig. 1A. During sliding ($8 < t < 11 \text{ hrs}$), F_N increased by nearly 20% and plateaued at higher velocities. F_S and μ increased initially, followed by a rapid decrease and an eventual increase at high sliding velocities. This monotonic frictional behavior is expected due to a stress-induced transition in the polymer chains near the sliding interface, as detailed in previous studies [45, 51]. In fact, we find excellent agreement between the rheology and tribology experiments when μ is plotted versus sliding velocity (Fig. S2). As in the tribology experiment, the post-sliding relaxation observed in Fig. 3A occurred over a similar timescale as the relaxation from the initial compression. This is evident of the bulk, hyperelastic swelling during sliding, and cannot be explained by local rehydration at the sliding interface.

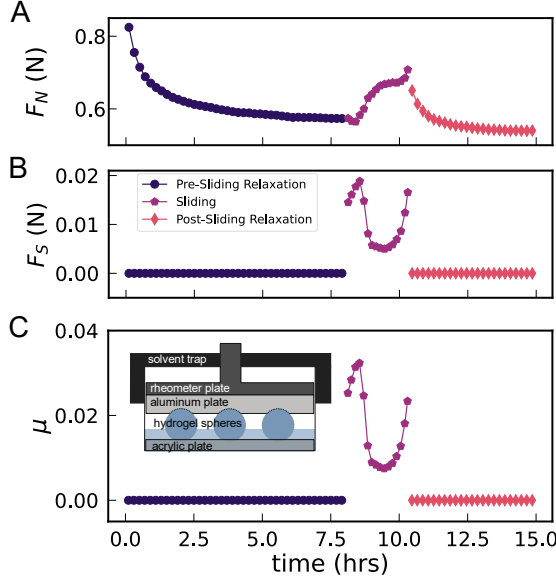


FIG. 3. Tough hydrogels exhibit a dilatant normal force upon sliding. Panels (A), (B), and (C) show the total normal force (F_N), shear force (F_S), and friction coefficient ($\mu = F_S/F_N$), respectively. The spheres underwent an 8-hour initial relaxation, a period of sliding at progressively increasing velocities (0.06 cm/s to 60 cm/s), and further relaxation post-sliding. The inset shows three PAA hydrogel spheres (diameter = 1.5 cm) placed at the vertices of an equilateral triangle and rotated by the upper rheometer plate while experiencing sliding against a smooth acrylic surface. Hydrogels were surrounded by a thin layer of water to ensure hydration.

IV. HYPERELASTIC DILATION FROM SIMPLE SHEAR

To further show that the dilatant effects observed during sliding are a bulk property, we used oscillatory rheology to quantitatively investigate the strain dependence predicted in Eqns. 1 and 2. We fabricated PAAm disks of thickness 6 mm and diameter 60 mm. The hydrogel disks were fully immersed in deionized water and placed between acrylic plates affixed with sandpaper to ensure a large static friction, as illustrated in Fig. 4A. The PAAm disks were initially compressed with a normal stress of ≈ 1800 Pa, corresponding to a normal strain of 5%, and then relaxed for 14 hours. Oscillatory strain sweep experiments were conducted over the range $0.01 \leq \gamma \leq 0.32$, spending 25 s per point. An oscillatory frequency of 1 Hz was chosen since it is much faster than the diffusive relaxation timescale. The change in normal stress, $\Delta\sigma_N$, is shown in Fig. 4B for multiple experiments and two different monomer concentrations. All data show remarkable agreement with $\sigma_N \propto \gamma^2$ (Eqn. 1) over more than a decade in strain.

Using Eqn. 1 and accounting for the average dilatant effect over the plate area (see SI), we found that R_v ranged from 13 kPa to 54 kPa. This coefficient can

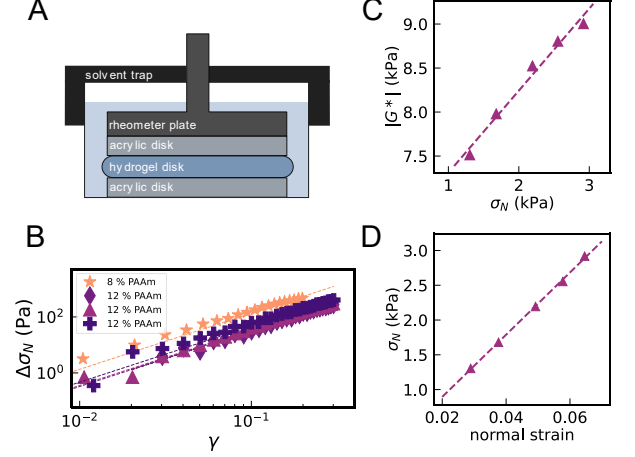


FIG. 4. Oscillatory rheology of hydrogels reveals a hyperelastic dilatancy. (A) Illustration showing a compressed PAAm disk of diameter 60 mm and thickness 6 mm between two acrylic disks. Sandpaper was glued to the acrylic to ensure no slip at the hydrogel interface. Each hydrogel disk was compressed with an initial normal stress and allowed to relax prior to testing. (B) The change in normal stress ($\Delta\sigma_N$) vs. strain (γ) for different hydrogel samples during an oscillatory strain sweep at 1 Hz. Each point is an average of 25 s spent at the corresponding strain. Dashed lines represent fitting results using the function $\Delta\sigma_N = R_v \gamma^2 / 4$ (Eqn. S8). (C) Complex modulus $|G^*|$ versus σ_N measured via oscillatory shear (1 Hz) at constant shear strain ($\gamma = 0.05$). (D) Normal stress versus normal strain. Young's modulus (E) can be calculated from the data (Eqns. S5-S6). For each point in (C-D), the hydrogel was relaxed to equilibrium 3 hrs before testing, and the dashed lines represent linear fits.

be theoretically described by Eqn. 2, which relies on Maxwell relations for the derivatives of elastic moduli in a hyperelastic material [39]. A hydrogel is necessarily more complex due to the coupling of the polymer network and poroelastic flow of the solvent, i.e., there are time dependent effects. Since the data from Fig. 4B starts from a fully-relaxed state of compression, we chose to measure the complex elastic shear modulus, $|G^*| = \sqrt{G'^2 + G''^2}$, and the Young's modulus, E , for fully relaxed hydrogels. Figure 4C-D shows $|G^*|$ as a function of σ_N , and σ_N as a function of the normal strain for a 12% PAAm gel. Assuming a linear relationship for both, we extracted $d|G^*|/d\sigma_N = 0.93$ and $E = 23.0$ kPa from the slopes of each fit, respectively. To account for viscoelasticity, $|G^*|$ was used instead of G [30], and the measurement of E accounted for the no-slip boundary conditions on the confining parallel plates (see SI) [52]. With these values, Eqn. 2 predicts $R_v = 13.1$ kPa. This should be compared to 14.2 kPa for the 12% PAAm hydrogel shown in Fig. 4B. The agreement is remarkable given that Eqn. 2 relies solely on elastic energy [39], whereas the free energy of a hydrogel contains both elastic and mixing free energies [42, 53]. We also emphasize that this pure dila-

tancy contrasts with prior studies of contractile ($R_v < 0$), low-modulus biopolymer gels [33, 35, 36, 38].

Previous experiments in low-modulus PAAm have shown that an initial dilatant normal stress can evolve to an eventual contractile stress over long times due to poroelastic flow [38]. We confirmed that this is not the case for tough PAAm hydrogels, and the dilatant behavior persists in equilibrium. First, we performed large-amplitude oscillatory shear and observed plastic deformation at long times, yet consistent dilatant behavior. Figure 5 shows time-sweep rheological measurements of a 12 % PAAm disk, which was compressed and relaxed for 14 hours prior to shearing. Oscillatory shearing was performed at 1 Hz at constant γ for 4 hours with constant normal strain. The normal stress was observed for an additional 4 hours post-shear. Figure 5A shows the shear stress, σ_S , of the hydrogel disk while the normal stress response, σ_N , is plotted in Fig. 5B, normalized by the normal stress value at $t = 14$ hrs ($\sigma_N(14)$). For $\gamma = 0.05$, σ_S remained constant over time, and σ_N increased by $\approx 15\%$ and plateaued. At $t = 18$ hrs (post-shear), σ_N quickly returned to its pre-shear value, $\sigma_N(14)$.

For strains larger than $\gamma = 0.05$, σ_S showed a slow increase over time, yet was non-monotonic with strain. The normal stress also exhibited purely dilatant behavior, increasing with time at large strains, and resulted in plastic deformations [54]. This can be seen during the post-shear regime, where σ_N relaxes to plateaus well below $\sigma_N(14)$. For $\gamma = 0.3$, this is more than 20% below $\sigma_N(14)$. The microscopic structural changes that result from such large strain are unclear, but are likely due to conformational changes of the polymer network since we observed no evidence of fracture. The plasticity at large strains is supported by measurements of the elastic modulus, G' , and the viscous modulus, G'' . Figure 5C illustrates that $G' > G''$ for small strains ($\gamma = 0.05$), and $G'' > G'$ for the largest strain ($\gamma = 0.30$). This is mainly due to the precipitous drop in G' , indicating changes to the polymer network, but not the average porosity.

To further demonstrate the robustness of dilatancy in tough hydrogels, we performed a second set of experiments applying *constant* shear stress and measuring the resulting creep and normal stress over hours. Figure 6A shows σ_S versus time for an 8% PAAm disk, which was compressed and relaxed for 14 hours prior to shearing using a setup identical to Fig. 4A. Shear stress was applied clockwise for 1 hour at each plateau, for a total of 6 hrs. Figure 6B shows that for small values of stress ($\sigma_S < 200$ Pa), γ increased proportionally and showed little to no time dependence. For larger stresses, γ increased dramatically over time, almost doubling after 1 hour at $\sigma_S = 300$ Pa (0th hour, 1st trial). This entire experiment was repeated in succession 4 times (Fig. S3), keeping the hydrogel compressed throughout, and the creep behavior eventually disappeared (138th hour, 1st trial). Importantly, during all experiments $\Delta\sigma_N$ was always positive (dilatant), and exhibited the same creep behavior as γ . Furthermore, we found that the com-

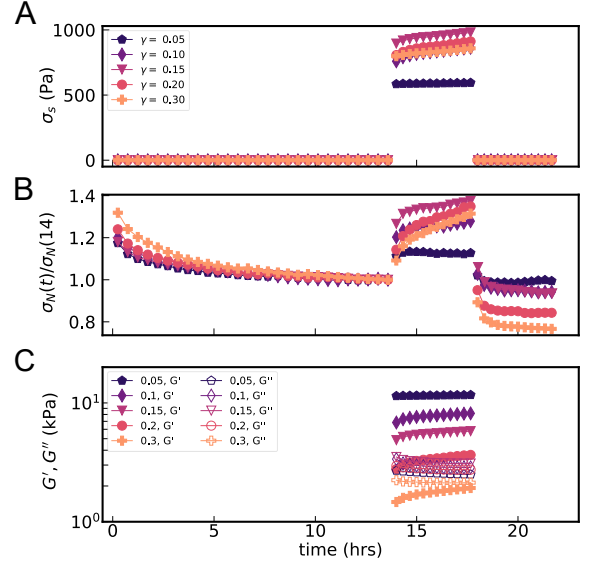


FIG. 5. Large strains introduce plastic changes in tough hydrogels. A 12% PAAm disk (diameter = 60 mm, thickness = 6 mm) was compressed with an initial normal stress of 2.0-2.5 kPa and allowed to relax. The experimental setup was identical to Fig. 4A. After compression, hydrogels experienced oscillatory shear at 1 Hz with strain amplitudes ranging from 0.05 - 0.3 for 4 hours, followed by subsequent relaxation. (A) The shear stress displayed a slow increase over time for larger strains. (B) The normal stress σ_N also experienced a significant increase over time at large strains. For each sample, σ_N has been scaled by its value at $t = 14$ hrs. After shearing, σ_N relaxed to asymptotic values well below $F_N(14)$, indicating plastic changes to the hydrogel network. (C) Storage (G') and loss (G'') moduli during oscillatory shear (14 hrs $< t < 18$ hrs). For small strains, $G' > G''$, whereas $G' \lesssim G''$ for the largest strain. All moduli decreased with increasing strain amplitude.

pression and shearing procedure introduced irreversible changes to the PAAm hydrogel. After the 1st trial shown in Fig. 6B, we allowed the fully-submerged PAAm disk to rest for 24 hours without confinement (a period that is longer than the poroelastic relaxation timescale). Upon re-compression and shearing (2nd trial), we found that the initial response was identical to the 1st trial, but the creep in γ and $\Delta\sigma_N$ observed at large σ_S was significantly reduced (Fig. 6B-C). Yet, after repeating experiment again (216th hour, 2nd trial), the behavior of γ and $\Delta\sigma_N$ aligned with the final state from the 1st trial.

Remarkably, although the hydrogel displayed consistent results after repeated shearing, we found that simply reversing the direction of shear on a subsequent experiment reintroduced creep in γ at large σ_S , as illustrated in Fig. 6B (246th hour, 2nd trial). We note that this approach to a steady behavior and sensitivity to directionality is reminiscent of “memories” observed simulations of sheared suspensions [55], and many other soft, complex

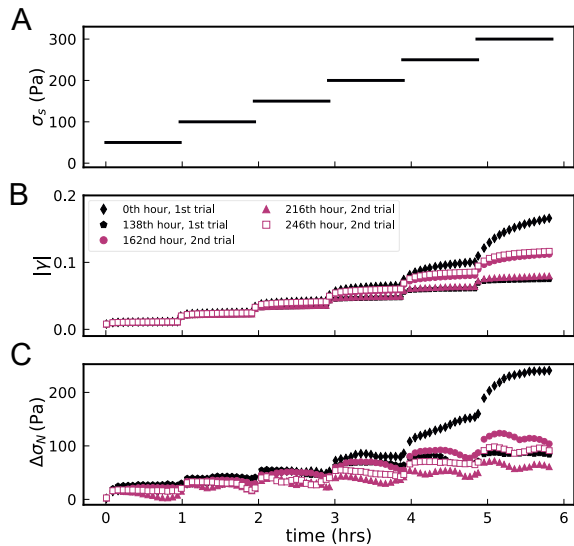


FIG. 6. Tough hydrogels display history-dependent behavior during creep. A series of linearly increasing (A) σ_S periods resulted in an increase in (B) γ and (C) $\Delta\sigma_N$ for an 8% PAAm hydrogel. Subsequent repetitions of the experiment produced a steady-state (Fig. S3). Removing the normal stress and allowing the hydrogel to recover for 24 hrs before repeating the experiment resulted in the return of observable (yet smaller) creep at large strains (magenta points). Strikingly, after reaching steady-state with little or no creep, simply reversing the direction of strain led to creep again, suggesting the hydrogel underwent plastic deformation with a memory of the strain direction. Closed symbols represent clockwise creep in all experiments, and open symbols represent counterclockwise creep.

systems [56]. We interpret the observed plastic behavior in PAAm as microscopic rearrangements of the polymer network that are irreversible, yet do not break existing covalent cross-links. This also means that the material will “remember” the largest applied signed strain, i.e., higher stress would lead to further creep. To quantify the creep behavior for $\sigma_S > 200$ Pa, we fitted each time series an power-law: $\gamma = C(t - t_0)^\alpha$, as shown in Fig. S4 A-B. The exponent α ranged from 0.22-0.52, reminiscent of Andrade-like creep [57]. Finally, for all experiments present in Fig. 6, we found that $\Delta\sigma_N$ did not follow the quadratic behavior suggested by Eqn. 1 (Fig. S4 C-D), which is expected due to the lack of time-dependence in the theory. Nevertheless, a positive dilatant effect was universally observed in all experiments presented here.

V. SUMMARY AND OUTLOOK

We provided compelling evidence that tough hydrogels exclusively dilate due to shear in both tribological and rheological experiments. The dilatancy can be explained by the bulk, hyperelastic properties of hydrogels. Specifically, the measured Reynolds dilation coefficient

(R_v) showed excellent agreement with leading order predictions from elasticity theory. Our results contradict prior experiments and theory suggesting purely contractile behavior in all hydrogels provided sufficient time has elapsed for poroelastic relaxation. These results may also explain the natural rehydration of stiff tissues such as cartilage during mechanical shearing, where dilation imbibes the surrounding synovial fluid. Given the contractile behavior observed in low-modulus gels, we expect the Reynolds coefficient R_v to change sign as the polymer network stiffens or softens. This transition should be related to the network micro-structure and cross-linking density. Additionally, the micro-structure can evolve over time and depends on shearing history, giving rise to plasticity and “memories” observed in creep experiments. These two directions remain exciting areas of research for future work.

ACKNOWLEDGMENTS

We acknowledge Daniel Sussman for insightful conversations, and Eric Weeks for use of the rheometer. This work was supported by the Gordon and Betty Moore Foundation, grant DOI 10.37807/gbmf12256.

VI. SUPPORTING INFORMATION

A. Hydrogel preparation

PAA (polyacrylic acid) and PAAm (polyacrylamide) hydrogels were used as model tough hydrogels. Commercial desiccated PAA spheres (Deco Beads, JRM Chemical, Inc.) were placed in de-ionized (DI) water and allowed to swell for 24 hours. The DI water was changed twice in the subsequent 48 hours to ensure the removal of free monomers and contaminants. PAAm hydrogels were prepared in two shapes: a sphere for tribology and compression measurements, and a disk for rheological shearing measurements. To make PAAm hydrogel solution, we combined DI water with a 29-1 acrylamide monomer and N,N'-Methylenebis(acrylamide) mixture (8-12 wt%), ammonium persulfate (0.05 wt%), and TEMED (0.1 wt%). All chemicals were purchased from Sigma Aldrich. The mixed gel solution was immediately poured into either a custom silicon spherical mold, or an acrylic disk mold. Polymerization occurred at room temperature for approximately 1 hour. Polymerized hydrogels were then immersed in DI water for 48 hours, and the water was changed every 24 hours to assist with removal of unpolymerized monomers and any contaminants.

B. Fitting Diffusion-Driven Relaxation Curves

In addition to Eqn. 4 in the main text, the following functional forms were used for fitting normal force relax-

ation curves of hydrogel spheres:

$$\frac{F_N(t) - F_\infty}{F_0 - F_\infty} = 1 - \frac{2.56(Dt/a^2)^\beta}{1 + 2.56(Dt/a^2)^\beta} \quad (\text{S1})$$

$$\frac{F_N(t) - F_\infty}{F_0 - F_\infty} = e^{-(Dt/a^2)^\beta}. \quad (\text{S2})$$

We obtained the contact radius a through optical exclusion microscopy, as done in prior work [45]. To obtain the Young's modulus (E), we measured the relationship between the contact radius and the applied normal force, as assumed that Hertzian contact theory is valid [45]:

$$a^3 = \frac{3F_0 R}{4E^*}. \quad (\text{S3})$$

Here, R is the hydrogel sphere radius and E^* is the hydrogel's reduced average modulus,

$$E^* = \frac{E}{1 - \nu^2}, \quad (\text{S4})$$

where ν is the Poisson's ratio. Knowing a , F_0 , and R , we calculated E^* of a PAA sphere by plotting F_0 vs. a^3 , as shown in Fig. S1. We obtained $E^* = 42.7$ kPa. Assuming that $\nu = 0.4$, the resulting Young's modulus is $E = 35.7$ kPa.

C. Interpreting Young's modulus and Reynolds coefficient from rheological measurements

When compressing a thin disk of elastic material in a parallel-plate rheometer, the ratio between the average normal stress (σ_N) and the normal strain (ξ) is not solely determined by the Young's modulus. If the material is allowed to freely slip along the plates and expand radially, then $d\sigma_N/d\xi = E$. However, if the material is fixed against the plates (i.e. with sandpaper) and cannot slip, then Poisson's ratio and the disk aspect ratio need to be considered. The slope of the normal stress versus normal strain is [52]

$$\frac{d\sigma_N}{d\xi} = E \frac{1 + 3\nu \left(\frac{1 - \nu}{1 + \nu} \right) S^2}{1 + 3\nu(1 - 2\nu)S^2}, \quad (\text{S5})$$

where $S = A/h$ is the aspect ratio of the gel disk, $A = 30$ mm is the disk radius, and $h = 6$ mm is the disk thickness. We also measure the shear modulus G , which is related to E and ν from linear elasticity theory:

$$E = 2G(1 + \nu). \quad (\text{S6})$$

With these two equations, we can solve for 2 unknowns: E and ν . For the 12% PAAm hydrogel disk shown in Fig. 4C-D in the main text, $E = 23.0$ kPa and $\nu = 0.4$.

The rheometer used in our experiments reports the maximum shear strain (γ_{\max}) at the edge of the parallel plate. In the main text, this is indicated as γ for

simplicity, i.e., Fig. 4B. However, hyperelastic dilation is a local phenomena, and care must be taken when interpreting rheometer measurements that are averaged over the plate. For example, assuming that the shear strain profile is linear in the radial direction, $\gamma_{\text{loc}} = \gamma_{\max} r/A$, where A is the radius of the rheometer plate. Assuming Eqn. 2 in the main text applies locally:

$$\Delta\sigma_N = \frac{1}{2} R_v \gamma^2, \quad (\text{S7})$$

correctly measuring R_v requires integrating over the area of the plate. Specifically:

$$\langle \Delta\sigma_N \rangle = \frac{1}{\pi A^2} \int_0^A \frac{1}{2} R_v \gamma_{\text{loc}}^2 2\pi r dr = \frac{1}{4} R_v \gamma_{\max}^2. \quad (\text{S8})$$

Thus, when measuring R_v from the fits shown in Fig. 4B, we used Eqn. S8, which includes a factor of $1/4$ instead of $1/2$.

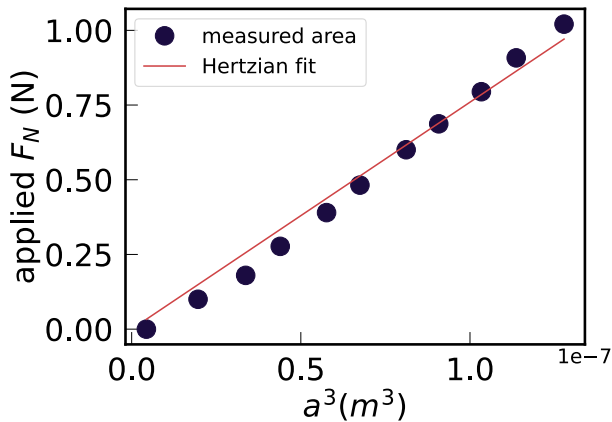


FIG. S1. Applied normal force versus a^3 for a PAA hydrogel sphere pressed onto an acrylic substrate. The data can be reasonably described by Hertzian contact theory, Eqn. S3. The red line represents a linear fit corresponding to $E^* = 42.7$ kPa, and thus $E = 35.7$ kPa (Eqn. S4). We note that the experiment was performed quickly so that diffusion-driven relaxation of the hydrogel was not important, in contrast to Fig. 1 in the main text.

-
- [1] S. D. Palanivelu, N. A. Z. Armir, A. Zulkifli, A. H. A. Hair, K. M. Salleh, K. Lindsey, M. H. Che-Othman, and S. Zakaria, Hydrogel application in urban farming: Potentials and limitations—a review, *Polymers* **14**, 2590 (2022).
 - [2] S. Mitura, A. Sionkowska, and A. Jaiswal, Biopolymers for hydrogels in cosmetics, *Journal of Materials Science: Materials in Medicine* **31**, 1 (2020).
 - [3] M. Sachdev, Y. Anantheshwar, B. Ashok, S. Hameed, and S. A. Pai, Facial granulomas secondary to injection of semi-permanent cosmetic dermal filler containing acrylic hydrogel particles, *Journal of Cutaneous and Aesthetic Surgery* **3**, 162 (2010).
 - [4] K. Y. Lee and D. J. Mooney, Hydrogels for tissue engineering, *Chemical reviews* **101**, 1869 (2001).
 - [5] J. L. Silverberg, A. R. Barrett, M. Das, P. B. Petersen, L. J. Bonassar, and I. Cohen, Structure-function relations and rigidity percolation in the shear properties of articular cartilage, *Biophysical journal* **107**, 1721 (2014).
 - [6] M. Hamidi, A. Azadi, and P. Rafei, Hydrogel nanoparticles in drug delivery, *Advanced drug delivery reviews* **60**, 1638 (2008).
 - [7] J. Li and D. J. Mooney, Designing hydrogels for controlled drug delivery, *Nature Reviews Materials* **1**, 1 (2016).
 - [8] C. A. Dreiss, Hydrogel design strategies for drug delivery, *Current opinion in colloid & interface science* **48**, 1 (2020).
 - [9] V. M. Sardinha, L. Lima, W. Belangero, C. Zavaglia, V. Bavaresco, and J. Gomes, Tribological characterization of polyvinyl alcohol hydrogel as substitute of articular cartilage, *Wear* **301**, 218 (2013).
 - [10] M. Parkes, C. Myant, D. Dini, and P. Cann, Tribology-optimised silk protein hydrogels for articular cartilage repair, *Tribology international* **89**, 9 (2015).
 - [11] M. M. Blum and T. C. Ovaert, Low friction hydrogel for articular cartilage repair: evaluation of mechanical and tribological properties in comparison with natural cartilage tissue, *Materials Science and Engineering: C* **33**, 4377 (2013).
 - [12] V. Bavaresco, C. Zavaglia, M. Reis, and J. Gomes, Study on the tribological properties of phema hydrogels for use in artificial articular cartilage, *Wear* **265**, 269 (2008).
 - [13] M. E. Freeman, M. J. Furey, B. J. Love, and J. M. Hampton, Friction, wear, and lubrication of hydrogels as synthetic articular cartilage, *Wear* **241**, 129 (2000).
 - [14] J. Kim and A. C. Dunn, Soft hydrated sliding interfaces as complex fluids, *Soft Matter* **12**, 6536 (2016).
 - [15] D. L. Burris and A. C. Moore, Cartilage and joint lubrication: new insights into the role of hydrodynamics, *Biotribology* **12**, 8 (2017).
 - [16] D. Burris, L. Ramsey, B. Graham, C. Price, and A. Moore, How sliding and hydrodynamics contribute to articular cartilage fluid and lubrication recovery, *Tribology Letters* **67**, 1 (2019).
 - [17] M. S. Farnham, R. E. Larson, D. L. Burris, and C. Price, Effects of mechanical injury on the tribological rehydration and lubrication of articular cartilage, *Journal of the Mechanical Behavior of Biomedical Materials* **101**, 103422 (2020).

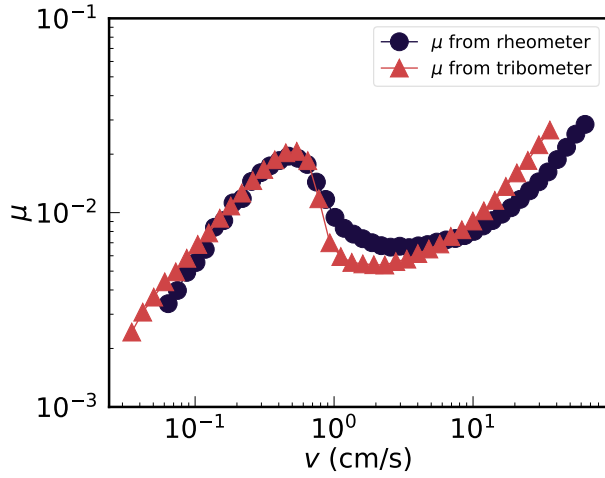


FIG. S2. Comparison between the measured friction coefficient μ from sliding PAA spheres using the rheometer and the tribometer. The frictional behavior from both measurement methods show good agreement, and agree well with previous measurements using the tribometer. Some discrepancies are expected due to variations between the 3 different PAA spheres used in the rheometer experiments. The non-monotonic behavior observed in the friction coefficient was discussed in detail in Cuccia et al. [45].

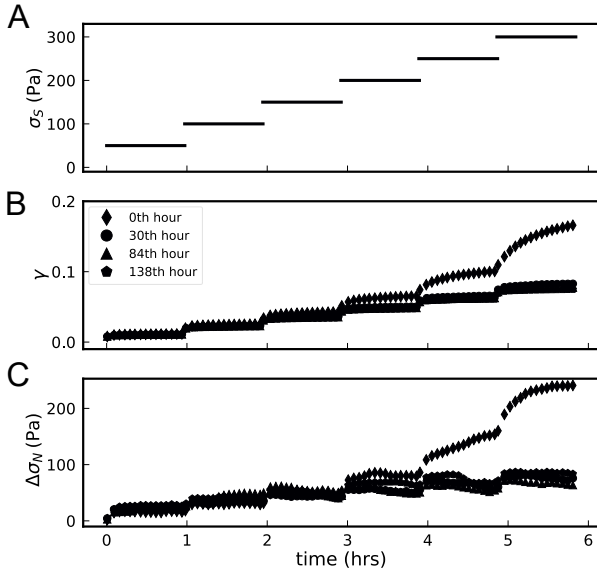


FIG. S3. A series of linearly increasing shear stress periods (1 hr each) resulted in an increase in shear strain and normal force. (A) The applied shear stress as a function of time and the resulted (B) strain γ and (C) normal stress difference $\Delta\sigma_N$. Significant creep was observed in both γ and $\Delta\sigma_N$ at large stresses. Each symbol represents a repetition of the experiment and the legend indicates when the experiment began with respect to the beginning of the first experiment. The normal strain was held fixed during and between all experiments.

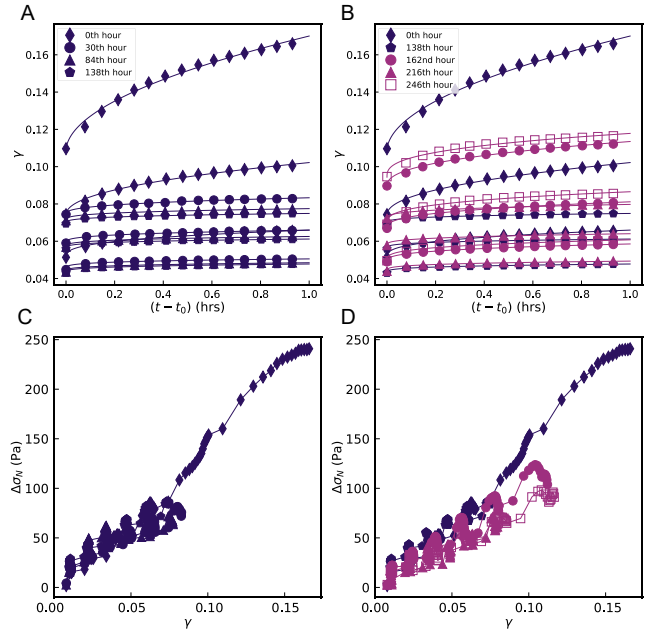


FIG. S4. Tough PAAm hydrogels are consistent with power law creep behavior, and display a non-quadratic dependence of σ_N versus γ when creep is present. (A) and (B) show power law fits of the form $\gamma = C(t - t_0)^\alpha$. The data shown is from Fig. S3 and Fig. 6 in the main text, and only for data that displayed significant creep ($\sigma_s \geq 200$ Pa). The exponent α ranged from 0.22 to 0.52. (C) and (D) show $\Delta\sigma_N$ vs. γ for all data during the creep experiments. Taken together, the quadratic relation between the normal force and strain, as shown in Fig. 4B in the main text at short times, is absent when creep and relaxation are present. However, the normal stress still increases for all data, corresponding a positive dilatant effect.

- [18] C. Putignano, D. Burris, A. Moore, and D. Dini, Cartilage rehydration: The sliding-induced hydrodynamic triggering mechanism, *Acta Biomaterialia* **125**, 90 (2021).
- [19] G. De Boer, N. Raske, S. Soltanahmadi, M. Bryant, and R. Hewson, Compliant-poroelastic lubrication in cartilage-on-cartilage line contacts, *Tribology-Materials, Surfaces & Interfaces* **14**, 151 (2020).
- [20] M. E. Kupratis, A. E. Gure, K. F. Ortvad, D. L. Burris, and C. Price, Comparative tribology: articulation-induced rehydration of cartilage across species, *Biotribology* **25**, 100159 (2021).
- [21] A. C. Moore and D. L. Burris, Tribological rehydration of cartilage and its potential role in preserving joint health, *Osteoarthritis and cartilage* **25**, 99 (2017).
- [22] J. Poynting, Xxxix. radiation pressure, *The London, Edinburgh, and Dublin Philosophical Magazine and Journal of Science* **9**, 393 (1905).
- [23] J. H. Poynting, On pressure perpendicular to the shear planes in finite pure shears, and on the lengthening of loaded wires when twisted, *Proceedings of the Royal Society of London. Series A, Containing Papers of a Mathematical and Physical Character* **82**, 546 (1909).
- [24] E. Billington, The poynting effect, *Acta mechanica* **58**,

- 19 (1986).
- [25] E. Vitral, Stretch formulations and the poynting effect in nonlinear elasticity, *International Journal of Non-Linear Mechanics* **148**, 104293 (2023).
 - [26] C. Horgan and J. Murphy, Poynting and reverse poynting effects in soft materials, *Soft matter* **13**, 4916 (2017).
 - [27] C. Horgan and J. Murphy, The effect of fiber-matrix interaction on the poynting effect for torsion of fibrous soft biomaterials, *Journal of the Mechanical Behavior of Biomedical Materials* **118**, 104410 (2021).
 - [28] J. L. Shivers, J. Feng, A. Sharma, and F. C. MacKintosh, Normal stress anisotropy and marginal stability in athermal elastic networks, *Soft Matter* **15**, 1666 (2019).
 - [29] S. Niroumandi, M. Shojaefard, and M. Baghani, Finite deformation of swollen pH-sensitive hydrogel cylinder under extension and torsion and its poynting effect: analytical solution and numerical verification, *International Journal of Applied Mechanics* **13**, 2150071 (2021).
 - [30] A. Fall, B. P. Tighe, and D. Bonn, Tuneable normal stresses in hyperelastic emulsions, *Physical Review Research* **4**, 013167 (2022).
 - [31] M. Mooney, A theory of large elastic deformation, *Journal of applied physics* **11**, 582 (1940).
 - [32] R. S. Rivlin, Large elastic deformations of isotropic materials iv. further developments of the general theory, *Philosophical transactions of the royal society of London. Series A, Mathematical and physical sciences* **241**, 379 (1948).
 - [33] P. A. Janmey, M. E. McCormick, S. Rammensee, J. L. Leight, P. C. Georges, and F. C. MacKintosh, Negative normal stress in semiflexible biopolymer gels, *Nature materials* **6**, 48 (2007).
 - [34] H. Kang, Q. Wen, P. A. Janmey, J. X. Tang, E. Conti, and F. C. MacKintosh, Nonlinear elasticity of stiff filament networks: strain stiffening, negative normal stress, and filament alignment in fibrin gels, *The Journal of Physical Chemistry B* **113**, 3799 (2009).
 - [35] M. Vahabi, B. E. Vos, H. C. De Cagny, D. Bonn, G. H. Koenderink, and F. MacKintosh, Normal stresses in semiflexible polymer hydrogels, *Physical Review E* **97**, 032418 (2018).
 - [36] E. Conti and F. C. MacKintosh, Cross-linked networks of stiff filaments exhibit negative normal stress, *Physical review letters* **102**, 088102 (2009).
 - [37] A. J. Licup, S. Münster, A. Sharma, M. Sheinman, L. M. Jawerth, B. Fabry, D. A. Weitz, and F. C. MacKintosh, Stress controls the mechanics of collagen networks, *Proceedings of the National Academy of Sciences* **112**, 9573 (2015).
 - [38] H. C. de Cagny, B. E. Vos, M. Vahabi, N. A. Kurniawan, M. Doi, G. H. Koenderink, F. C. MacKintosh, and D. Bonn, Porosity governs normal stresses in polymer gels, *Physical review letters* **117**, 217802 (2016).
 - [39] B. P. Tighe, Shear dilatancy in marginal solids, *Granular Matter* **16**, 203 (2014).
 - [40] K. Baumgarten and B. P. Tighe, Normal stresses, contraction, and stiffening in sheared elastic networks, *Physical review letters* **120**, 148004 (2018).
 - [41] O. Reynolds, Experiments showing dilatancy, a property of granular material, possibly connected with gravitation, *Proc. R. Inst. GB* **11**, 12 (1886).
 - [42] M. Doi, Gel dynamics, *Journal of the Physical Society of Japan* **78**, 052001 (2009).
 - [43] M. Doi and S. Edwards, Dynamics of concentrated polymer systems. part 1.—brownian motion in the equilibrium state, *Journal of the Chemical Society, Faraday Transactions 2: Molecular and Chemical Physics* **74**, 1789 (1978).
 - [44] J.-F. Louf and S. S. Datta, Poroelastic shape relaxation of hydrogel particles, *Soft matter* **17**, 3840 (2021).
 - [45] N. L. Cuccia, S. Pothineni, B. Wu, J. Méndez Harper, and J. C. Burton, Pore-size dependence and slow relaxation of hydrogel friction on smooth surfaces, *Proceedings of the National Academy of Sciences* **117**, 11247 (2020).
 - [46] J. D. Berry, M. Biviano, and R. R. Dagastine, Poroelastic properties of hydrogel microparticles, *Soft Matter* **16**, 5314 (2020).
 - [47] Y. Hu, X. Zhao, J. J. Vlassak, and Z. Suo, Using indentation to characterize the poroelasticity of gels, *Applied Physics Letters* **96** (2010).
 - [48] Z. I. Kalcicoglu, R. Mahmoodian, Y. Hu, Z. Suo, and K. J. Van Vliet, From macro-to microscale poroelastic characterization of polymeric hydrogels via indentation, *Soft Matter* **8**, 3393 (2012).
 - [49] S. Cuenot, P. Gélébart, C. Siquin, S. Collic-Jouault, and A. Zykwinska, Mechanical relaxations of hydrogels governed by their physical or chemical crosslinks, *Journal of the mechanical behavior of biomedical materials* **133**, 105343 (2022).
 - [50] M. H. Esteki, A. A. Alemrajabi, C. M. Hall, G. K. Sheridan, M. Azadi, and E. Moeendarbary, A new framework for characterization of poroelastic materials using indentation, *Acta biomaterialia* **102**, 138 (2020).
 - [51] B. Wu, J. M. Harper, and J. C. Burton, Relaxation and recovery in hydrogel friction on smooth surfaces, *Experimental Mechanics* **61**, 1081 (2021).
 - [52] J. Williams and C. Gamonpilas, Using the simple compression test to determine young's modulus, poisson's ratio and the coulomb friction coefficient, *International Journal of Solids and Structures* **45**, 4448 (2008).
 - [53] P. J. Flory and J. Rehner Jr, Statistical mechanics of cross-linked polymer networks ii. swelling, *The journal of chemical physics* **11**, 521 (1943).
 - [54] E. Ban, J. M. Franklin, S. Nam, L. R. Smith, H. Wang, R. G. Wells, O. Chaudhuri, J. T. Liphardt, and V. B. Shenoy, Mechanisms of plastic deformation in collagen networks induced by cellular forces, *Biophysical journal* **114**, 450 (2018).
 - [55] N. C. Keim and S. R. Nagel, Generic transient memory formation in disordered systems with noise, *Physical review letters* **107**, 010603 (2011).
 - [56] N. C. Keim, J. D. Paulsen, Z. Zeravcic, S. Sastry, and S. R. Nagel, Memory formation in matter, *Reviews of Modern Physics* **91**, 035002 (2019).
 - [57] E. N. D. C. Andrade, On the viscous flow in metals, and allied phenomena, *Proceedings of the Royal Society of London. Series A, Containing Papers of a Mathematical and Physical Character* **84**, 1 (1910).